Solid-State Metal Additive Manufacturing: A Review

NIHAN TUNCER [ID][1,2,3] and ANIMESH BOSE[1]

1.—Desktop Metal, Inc., 63 Third Ave, Burlington, MA 01803, USA. 2.—e-mail: nihantuncer@gmail.com. 3.—e-mail: nihantuncer@desktopmetal.com

Although a significant amount of technical, commercial, and academic resources have been invested in laser and electron beam-based additive manufacturing (AM) of metals and alloys over several decades, challenges and limitations associated with repeated local melting and processing complexity along with the cost of equipment and operation have sparked interest in research on solid-state AM methods as an alternative. This paper reviews the capabilities and challenges of major solid-state metal AM techniques by dividing it into two broad categories (plastic deformation based and sinter based) depending on the metallurgical bonding mechanisms, range of processible alloys, and resulting microstructures. The limited and recent data available in literature show that, while deformation-based AM techniques are primarily limited to relatively ductile alloys, a larger variety of materials are suitable for manufacturing through sinter-based AM. Deformation-based methods generally refine the microstructure by recrystallization, while in most cases sinter-based AM methods lead to grain growth due to high-temperature processing and a more isotropic microstructure. Among the solid-state AM methods summarized here, the binder jetting and additive friction stir AM methods stand out with isotropic microstructures and mechanical properties close to the wrought properties.

INTRODUCTION

Additive manufacturing (AM), also commonly referred to as three-dimensional (3D) printing, allows layer-by-layer building of complex shaped parts from engineering materials without the use of tooling. A myriad of engineering materials, such as polymers, polymer-matrix composites, ceramics, metals and alloys, and metal- and ceramic-matrix composites, have been fabricated using various 3D printing methods.[1–7] The early commercial applications of 3D metal printing were laser-based technologies. The advancement of laser technologies and the development of electron beam processing led to the proliferation of commercial AM technology. Developments of commercial 3D printing started around the 1980s, with early demonstration being based on curing of photopolymers by ultraviolet lasers that formed the basis of 3D Systems Corporation. This was soon followed by 3D printing by melting of powdered feedstocks using laser beams. The ability of 3D printing to create viable commercial metal alloys was brought to the limelight by the General Electric Aero LEAP fuel nozzle that combined 18 components into a single one using laser beams.[8] Electron beam (EB)-based technologies followed, enabling the fabrication of several different high-temperature metals and alloys.[9] Though the early commercial applications of metal 3D printing used beam-based technologies, these technologies are expensive, require well-qualified operators to run the machine, have relatively low productivity, and need expensive powders with specialized powder size distribution and low oxygen content. Also, all beam-based technologies result in the final part being welded to the base plate, requiring extensive postprocess machining, which along with the extensive facility requirements make the investment for beam-based technologies too expensive, resulting in slow adaptation of 3D printing into mainstream manufacturing.

Beyond the economical and practical challenges summarized above, the quality of the parts produced by beam-based AM technologies also needs to be improved. Such processes are prone to solidification-related defects such as residual stress,

distortion, elemental segregation, volatile element loss, hot cracking, and porosity.[2,10] The spatially variable thermal cycles result in inhomogeneous microstructure and properties. Moreover, it is challenging to process nonweldable alloys and alloys with complex metallurgy such as precipitation-hardening alloys, some tool steels, and cermets using beam-based AM technologies. These challenges could potentially be overcome by additive manufacturing in solid state. This has led to the proliferation of myriad non-beam-based, solid-state AM technologies for metals and alloys.

With the ever-increasing interest in and rapid evolution of AM technologies, a large number of review articles focusing on a specific solid-state AM technique,[11–14] a specific material class,[15–19] and comparative analyses of multiple additive manufacturing methods[2,4,20,21] have been published. This review presents an alternative classification of solid-state AM methods based on the bonding mechanism and its effect on the microstructure and mechanical properties of the resulting components. Although a large number of solid-state AM technologies are currently being explored, only a handful of them have shown some commercial potential yet. This review discusses six solid-state AM technologies, three based on sintering and three based on mechanical deformation techniques: binder jetting, material extrusion, screen or stencil printing, ultrasonic, friction stir, and cold spray AM. The first part of the review describes the classification approach, followed by a second section where a detailed description of each technique is presented. A critical analysis and comparison between the different technologies, from the points of view of the processible materials, geometric capabilities, microstructure, mechanical properties, anisotropy, and chemistry, are presented in the final section.

CLASSIFICATION OF SOLID-STATE AM TECHNOLOGIES

ISO/ASTM 52900 classifies AM processes into seven categories, comprising binder jetting, directed energy deposition (DED), powder bed fusion (PBF), material extrusion, material jetting, sheet lamination, and vat photopolymerization.[22] While this categorization has more of a discrete nature, ISO/ASTM 52900, among the many ways used to classify AM processes, also classifies AM techniques based on two broad process characteristics, viz. singe- and multistep techniques.

It is worth emphasizing that the capabilities, challenges, and resulting material properties of each AM technology largely depend on the layer bonding method and consolidation mechanism. When these aspects are considered, two main categories emerge: beam-based methods that rely on material bonding by local melting, and solid-state AM techniques where the material remains solid (Fig. 1). It should be mentioned that some of the solid-state AM techniques could include some fraction of liquid-phase formation during the consolidation stage, but this will be considered as solid-state AM in this review. Beam-based techniques including powder bed fusion (PBF) and direct energy deposition (DED) lie beyond the scope of this review.

Solid-state AM methods for metals and alloys, which is the focus of this review, can be divided into two subcategories, primarily based on the material bonding method. Sintering-based solid-state additive manufacturing is characterized by consolidation of a 3D-printed powder compact via uniform external heating up to a high fraction of the melting temperature, i.e., sintering. The externally applied thermal energy increases the total system energy, causing the material to reduce its total surface area by material bonding. Material bonding occurs through atomic diffusion between metal powder particles, which is generally facilitated by thermal reduction of the oxide layer on powder surfaces. Binder jetting (BJAM), metal extrusion AM (MEAM), and screen or stencil 3D printing (SPAM) fall into this category. Sintering-based AM techniques offer the advantage of leveraging the mature knowledgebase on powder metallurgy and sintering technology.[23,24]

The second category of solid-state AM is mechanical deformation (MD)-based techniques, in which mechanical disruption of the oxide layer is followed by material bonding through severe plastic deformation, which can be induced by ultrasonic scrubbing, friction, or supersonic impact of powder particles onto a substrate or a previous layer of the same material. Ultrasonic additive manufacturing (UAM), additive friction stir (AFSD), and cold spray (CSAM) processes fall into this category. These techniques use mechanical energy to facilitate metallic bonding.

Sintering-Based AM Processes

Sintering-based additive manufacturing techniques are multistep processes where the initial geometry building is separate from the consolidation step. The first operation produces an oversized geometry of the desired part by "gluing" together metal powder particles into a free-form 3D preform using polymeric binders, followed by a step that cleanly removes the organic binders (generally referred to as debinding), which is followed by the final consolidation of the part through sintering. The sintering step often serves multiple purposes that include development of the desired physical and mechanical properties, achievement of the final dimensions of the part (shrinkage is associated with sintering), and in some cases achieving chemical homogenization (starting initially with an elemental powder mixture that ends up as a homogeneous alloy after sintering). Sintering is a thermal
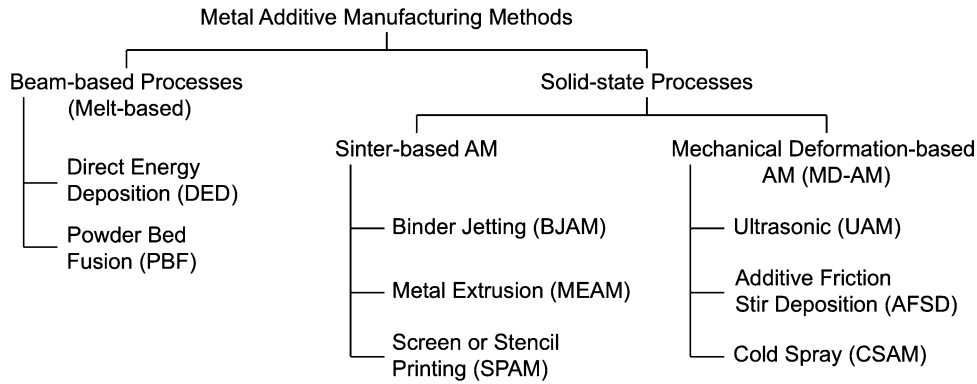
Fig. 1. Classification of additive manufacturing processes based on material bonding methods. This review covers only the processes outlined as solid-state processes.
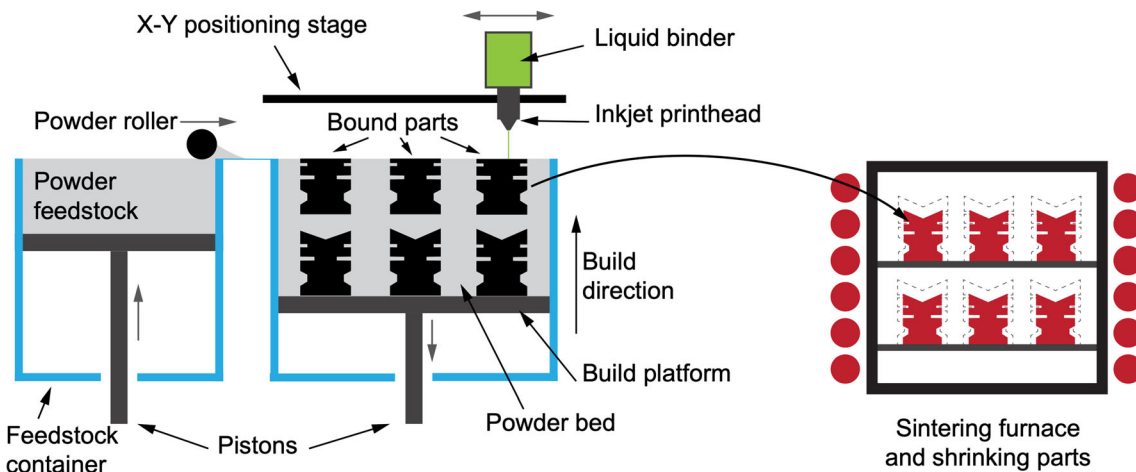

Fig. 2. Schematic of printing and sintering steps of BJAM.

treatment where material bonding occurs through atomic diffusion between powder particles, which is generally facilitated by oxide reduction at high temperature and preferentially under an atmosphere with low oxygen partial pressure. The driving force for sintering is reduction of the surface area of the powder.[23] It is important to note that, although we classify sinter-based methods under the solid-state AM category, the sintering process may also include liquid-phase sintering, where a small fraction of the material forms a liquid phase during the sintering process (e.g., hard metals, heavy alloys, some tool steels, etc.).

Binder Jetting (BJAM)

Binder jetting is a sintering-based AM technique where a 3D geometry is built up layer by layer through the spreading of a thin powder layer (typically between 50 μm and 200 μm) in a confined bed followed by spraying of an organic binder, which is generally dissolved in a solvent, on the desired areas through the use of a moving printhead with numerous nozzles (Fig. 2). This causes the areas

that are sprayed with the binder to bond while the surrounding powder particles remain loose. The powder is generally transferred from a powder holding bin into a build box using a roller or less commonly a doctor blade, which spreads the next layer of the powder onto the build box. The binder not only spreads on the X–Y plane (along the print bed plane) but also into the powder layer below each successive powder layer. This results in the integration of the layers not only in the X–Y plane but also along the build direction (Z-direction). Once the binder has been sprayed on an individual powder layer, a piston in the feedstock container is pushed up to a desired level and the build box is shifted downward along the Z-direction (based on the desired layer thickness). Generally, after printing each layer, the solvent is rapidly removed while the next powder layer is spread. The 3D part built in this way is fragile at this stage, as it is held together by the organic binder and supported by the loose powder surrounding it. The build box along with the fragile parts and the surrounding loose powder are then introduced into a low-temperature curing oven. The organic binder generally crosslinks on

the application of thermal energy, strengthening the part prior to separation from the loose powder (depowdering). After depowdering, the 3D preform that comprises metal powder particles bound by crosslinked binder with porosity of 40% to 50%[11] goes through subsequent thermal debinding and sinter steps in an atmosphere-controlled furnace. Sometimes, the thermal debinding and sintering steps are carried out in different furnaces, while in other cases they are achieved in the same furnace.

Binder jetting can be used to process almost any material that comes in the desired powder form and be consolidated through subsequent treatments such as sintering that can be followed by containerless hot isostatic pressing (HIP) and/or heat treatment. This flexibility in terms of processible materials and the potential for high speed, large volume production has populated the commercial space with companies developing binder jetting machines and advancing commercialization of the technology, such as ExOne, HP, Digital Metal, and Desktop Metal. Common examples of materials that can be additively manufactured through binder jetting described in literature and available from the aforementioned companies include a variety of precipitation-hardening and austenitic stainless steels, tool steels, Ti-6Al-4V, Inconel 625 and 718, and copper.[25–28]

The success and properties of the resulting builds are dependent on a large number of processing variables. Some of the major process variables include the powder characteristics (shape, size and distribution, and chemistry), the condition of the powder (surface oxides and contamination, moisture content of the powder bed, and fresh or recycled powder), the spreading uniformity and green density of the powder layer (dictated by the rpm of the roller and the roller travel speed, as well as the ability of the powder to be spread), the curing temperature, the surface tension of the binder, the saturation level (described as the fraction of void space between the powder particles that is filled by the binder), the amount of powder in front of the counter-rotating roller, the roller diameter, the surface condition of the roller, the material that the roller is made from, the volume of the binder droplet, the velocity of the droplet as it meets the powder bed, the number of nozzles over a fixed length, the nozzle orifice diameter, the standoff distance between the nozzles and the powder bed, and the debinding and sintering parameters (thermal cycles and the debinding and sintering atmosphere). Along with all the abovementioned process variables, the environmental and safety aspects of the powder spreading and handling processes must also be considered, making it necessary to test for powder explosivity and toxicity.

In the conventional binder jet process, the powder is transferred from the powder holding box to the build box. This results in a large mound of powder that is initially in front of the counter-rotating roller that moves to spread the powder from one end of the build box to the other. Thus, the powder mound in front of the roller is continually reduced as the roller travels along the length of the build box. This can lead to nonuniformity in the powder bed density, which results in nonuniform shrinkage and distortion of the part.[29] To reduce this nonuniformity and increase the efficiency and speed of the process, a variation of the binder jet process named single-pass jetting (SPJ) was developed at Desktop Metal. SPJ relies on bidirectional printing where all the steps of the printing process, i.e., powder deposition, spreading, compacting, ballistic suppression (the ability to suppress powders from the powder bed to be ejected and deposited on the nozzle orifice), and binder jet printing, are executed by a moving platform on each pass over the build area.[26] Continuous dispension of the powder in front of the rotating roller creates a uniform powder mound that is always present as it traverses the entire length of the powder bed, resulting in a uniform powder bed density.

Parts manufactured by binder jetting are consolidated by a sintering process, which dictates their final density, shrinkage, and mechanical properties. Due to their large surface area and thus high driving force for consolidation, fine powders are typically preferred for sintering. The flowability of the powders, which controls the uniform spreading on the powder bed, on the other hand, is typically inversely proportional to the powder size due to the interparticle forces between fine powder particles. Any nonuniformity in the powder bed, such as agglomeration and segregation based on powder size, will result in differential shrinkage during sintering, leading to part distortion, warping, and/ or cracking. The powder size and distribution also affect the binder saturation levels.[11] While the typical powder size used in binder jetting of various metals varies between 20 μm and 80 μm, numerous studies have been studied on the ideal powder size and distribution that satisfies most requirements.[30–34] Finer cuts and multimodal powder sizes are reported to enhance the green and final densities and improve the surface finish. However, challenges associated with powder bed nonuniformity, inhomogeneous pore distribution, and distortion in complex geometries due to segregation in multimodal powder feedstocks have not been adequately addressed. Another requirement for flowability is powder morphology. Typically, powders with smooth surfaces provide an uninterrupted flow, thus spherical powders are preferred for binder jetting, as they flow better than irregular-shaped ones.[11]

Alternative approaches to achieve high densities while allowing the use of large flowable powders include infiltration and the use of sintering aids. Partial sintering of the binder-jetted part to $\sim 50\%$ density followed by infiltrating it with a low-melting alloy that can wet the matrix material has been shown to yield densities above 95%. Examples

include infiltrating steel with bronze,[35,36] WC with Co,[37] and B_4C with Al.[38] Addition of very small amounts of boron-based sintering aids has also been shown to improve the densification of binder-jetted 316L parts.[39]

Material Extrusion-Based Additive Manufacturing (MEAM)

The process of material extrusion, the most common type of which is fused filament fabrication (FFF), was originally developed by Stratasys in 1989.[40] It is based on extrusion of a thermoplastic polymer through a heated nozzle with a fine orifice onto a substrate to build a free-form 3D structure layer by layer. The extrusion-based metal AM process was born when a well-known manufacturing method, metal injection molding (MIM), where metal or ceramic powders bound with polymeric binder are pushed into a mold, was adapted to produce metal components from FFF green parts.[41]

As in MIM, the MEAM process typically uses metal or alloy powders mixed with multicomponent organic binders as feedstock. The raw material in this process is generally in the form of a flexible filament coiled onto a spool or discreet rods (as used by most of FFF fabricators such as Fraunhofer IFAM and MarkForged) loaded into a cartridge as in bound metal deposition (BMD), a variation of MEAM developed by Desktop Metal. The multicomponent binder system typically consists of a primary component that can be removed early on, and a secondary binder that remains to hold the part shape until it is consolidated thermally by sintering. The primary binder can be removed using techniques including dissolving in a solvent, thermal wicking, supercritical extraction, or sublimation, which opens the way for the remaining secondary binder component to be removed thermally in a furnace. The secondary binder is thermally removed immediately around the onset of necking between the powder particles but before the formation of closed porosity. Other organic additives are used as viscosity modifiers.

The process begins with extrusion of the feedstock through a nozzle onto a print bed to build a free-form 3D structure layer by layer. A unique feature of this process is that it allows the use of multiple extrusion mechanisms, i.e., printheads, that are fed with different material feedstocks, thereby facilitating multimaterial printing. The parallel extrusion mechanisms are attached to a moving gantry (Fig. 3a). In each extruder, a preformed rod of feedstock is forced into a cavity in which it is heated beyond the softening temperature of the thermoplastic binder and dispensed through an orifice. The process relies on dispensing the extruded material at a temperature where it is in a state that it can strongly adhere to the previously laid extruded layer and form a good bond. Once laid, the extrudate must immediately solidify and gain shape stability

before the next extruded layer is dispensed on top. After printing of the thermoplastic composite part, a significant fraction (30% to 70%) of the organic binder is removed generally by chemical dissolution, which is commonly referred to as "solvent debinding," leaving the powder held together by a secondary binder component with interconnected porosity throughout the part. This interconnected porosity provides a pathway to the surface for the remaining binder to be removed in the subsequent thermal debinding. The remaining portion of the binder is removed thermally in the first stage of heat treatment (often known as thermal debinding and presintering), which is followed by sintering (typically at temperatures above 75% of the melting point of the metal or alloy). Therefore, the bonding mechanism is atomic diffusion between powder particles at high temperature, as in BJAM.

The critical parameters that control the density and strength of the build are feedstock parameters (flow characteristics of the binder, metal powder size, morphology, and volume fraction of the solid in the feedstock), print parameters (nozzle temperature, layer height and width, cooling fan speed, toolpathing, and track width), and debinding and sintering parameters (furnace atmosphere and thermal cycle).[42] The mesostructure of the printed parts is derived from the placement and morphology of the extruded tracks, which is preserved throughout debinding and sintering. The feedstock and print parameters must be adjusted to ensure full layer adhesion to avoid any delamination that may occur in the following stages of the process. The volume of the extruded material should overfill the spacing between the printhead tracks in order to achieve full-density parts (Fig. 3b).[43,44] Toolpath optimization is also required to eliminate large voids in the printed parts and minimize the anisotropy arising from the orientation of the tracks.

An important factor that must be considered when printing dense structures is that the thicker cross sections require more time to complete the solvent and thermal debinding stages without damaging the part geometry. Removal of the binder components starts on the surface and progresses towards the core of the part as porosity forms in the outer shell by dissolution (in solvent debinding) or evaporation (in thermal debinding) of the binder components. In solvent debinding, the porosity allows the solvent to diffuse into the porous compact and come into contact with the next layer of the primary binder component. The time required for this successive process increases with increasing thickness. In thermal debinding, the secondary binder that melts and evaporates must diffuse towards the surface and escape through the open porosity before pressurizing the voids in the powder compact. Parts that have dense cross sections exceeding a few millimeters require long debinding times and carry the risk of part deformation and cracking in cases where the binder evaporation or
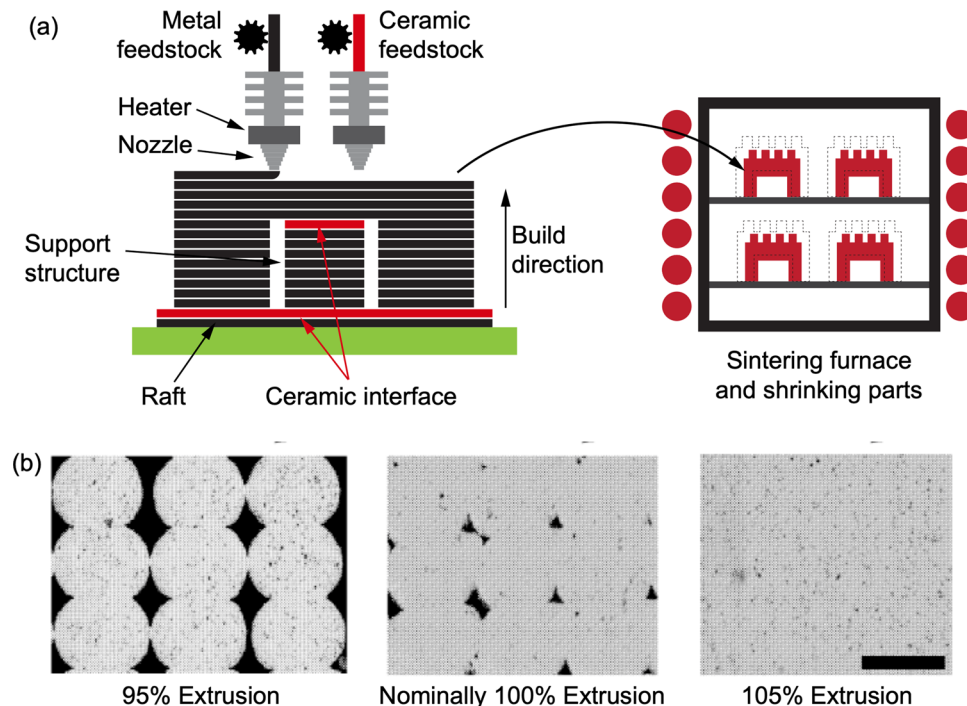
Fig. 3. (a) Schematic representation of MEAM where binder–powder feedstock is deposited by extrusion through a nozzle layer by layer followed by debinding and sintering. The primary debinding step is not shown. Support structures and raft are separated from the part using a ceramic separation layer. (b) Effect of layer dimensions and extrusion percentage on density of the prints in MEAM. The micron bar is about 400 μm. Reprinted from Ref. 43.

expansion rate is much higher than the removal rate.[42]

In contrast to binder jetting, in MEAM the flow and deposition characteristics of the feedstock, and thus its printability, are controlled primarily by the viscosity of the binder and the printing temperature. Therefore, powder characteristics do not pose a significant limitation, unless using coarse spherical powders with low interparticle friction that can result in slumping when the binder is removed. Any metal or ceramic that can be consolidated through sintering can be 3D printed through MEAM. Materials that have been successfully printed include stainless steels, tool steels, low-alloy steels, Inconel, copper, and WC–Co.[26,42,45–48] The ability of this process to fabricate exotic materials has also been demonstrated through the fabrication of novel WCr- and NiCr-based nonequilibrium alloys.[49]

In addition to this vast material selection, a significant advantage of EAM is the ease of fabrication of complex geometries with supports, overhangs, infills, enclosed channels, and multicomponent assemblies thanks to the separable interface layer that enables easy separation of the support from the part. The interface layer is printed using a second nozzle and is retained throughout the process, including the sintering stage, where the ceramic is not consolidated (turning back into particulates). During sintering, the special ceramic separation layer creates a barrier that prevents metallurgically bonding of the part to the support
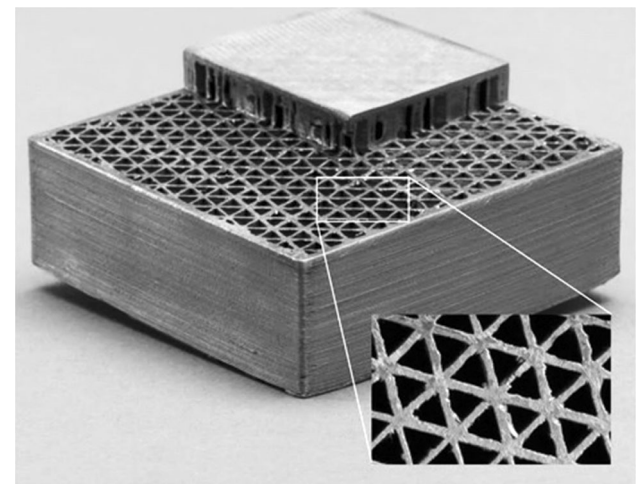

Fig. 4. Machined part revealing the infill structure along with the parameter wall, produced by Desktop Metal.

structure, enabling easy separation. The separation layer is also used to separate the part from the "raft," which is a substrate printed from the same material that shrinks at the same rate as the part to prevent part distortion due to the friction between the part and the sintering substrate during sintering.[26] Another unique advantage of the MEAM process is its ability to print internal latticework infill structures, which drastically reduces the
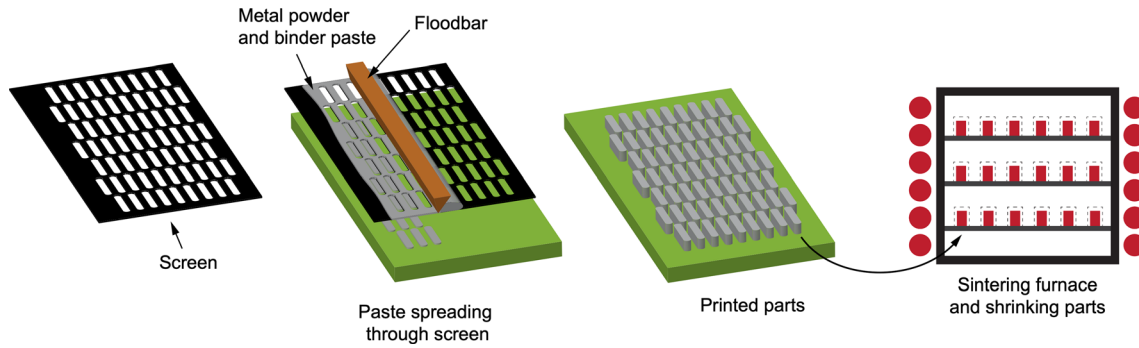
Fig. 5. Schematic of overall processing steps for screen/stencil 3D printing. A high-viscosity metal powder/binder paste is spread and pushed through a screen layer by layer.

processing time as well as resulting in parts that are lightweight (Fig. 4).

Some of the disadvantages of this process include the slow nature of the build, which does not lend itself to mass production, and the relatively poor surface finish compared with some other metal AM printing technologies.

Screen and Stencil 3D Printing (SPAM)

The third sinter-based AM technique is screen or stencil printing, which uses pastes created by mixing metal or alloy powders with organic or aqueous solvent-based slurries. A schematic of the printing process is shown in Fig. 5. The screen is located slightly above a substrate on which the part is printed. The screens can be fabricated as a negative of the part design, while stencils are typically cut by a laser from sheet metal. Once the floodbar has spread the paste over the screen, a printing squeegee bar pushes on the paste, which then presses on the screen and squeezes material through in places where the screen mesh has openings. The paste used generally exhibits shear thinning during the processing step. The substrate on which the layer of paste is deposited is transported out of the printing chamber and quickly dried to remove the solvents before the next layer can be printed. For printing of the next layer, the screen or stencil is lifted in the Z-direction by a distance that represents the layer height (known as the snapoff distance). The typical layer height for 3D screen printing is 5 μm to 15 μm,[50] while in the case of 3D stencil printing the layer height can be in the range of 300 μm to 500 μm. The part created is a "green" part that has some amount of organic binder (between 2% and 5%) that is retained and some open porosity that allowed the removal of the solvent. This green part must be sintered in a furnace to densify it. A large number of process variables govern the print quality. The most critical ones are the paste properties (viscosity, particle loading), snapoff distance that dictates the layer height, aperture design, squeegee pressure, and traverse speed, among others.[51,52]

High-resolution, complex geometry builds have been produced by screen and stencil printing from 316L, 17-4PH stainless steels, Cu, Ti alloys, and ceramic–metal composites.[53,54]

Typically, the particle size must be less than a third of the size of the orifices in the screen. Thus, to improve the part resolution, finer powders are preferred. The particle loading in the paste must be between 20 vol.% and 45 vol.% to avoid undesired shear thickening during the process.[50] The process is capable of making parts that have different materials in different layers or sometimes even different materials in the same layer. Screen or stencil printing, which is generally used to create fairly small-sized parts in very high volumes, is capable of printing millions of small-sized parts, thus making it suitable for mass production of small parts, generally with limited changes in the geometry along the Z-direction as it requires the use of different screens or stencils, which can be relatively expensive.

Mechanical Deformation-Based Additive Manufacturing (MD-AM) Methods

The main characteristic that separates MD-AM techniques from sinter-based ones is that, while sinter-based AM methods provide thermal energy as the driving force for material bonding, this second category of solid-state AM techniques employ kinetic energy to facilitate bonding. The kinetic energy can be administered by high-frequency ultrasonic waves or rotational friction accompanied by a normal force, or supersonic impact. Heat is a byproduct of the process, and the extent of the local temperature rise depends on the physical and thermal properties of the material that is being built as well as the substrate material. The microstructures of components manufactured via MD-based processes are characterized by recrystallized fine grains in regions where severe plastic deformation occurs. The general principles of the three major MD-AM methods, namely UAM, AFSD, and CSAM, are summarized in this section.
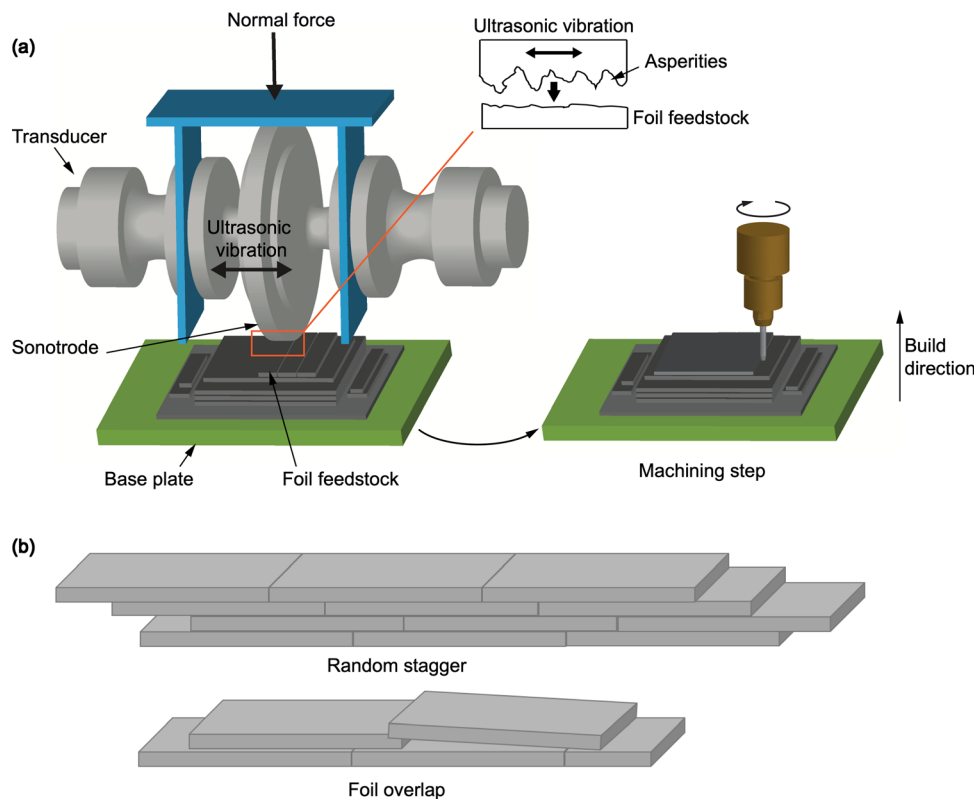
Fig. 6. (a) Schematic of UAM and machining steps where metal foils are joined by high-frequency ultrasonic vibrations with subsequent machining step. (b) Schematic illustration of tape staggering and overlap to minimize weld-line voids.

Ultrasonic Additive Manufacturing (UAM)

Ultrasonic additive manufacturing is a solid-state AM process where a stack of similar or dissimilar metal foils are joined by high-frequency (typically 20 kHz) ultrasonic vibrations while a normal force is also applied, interrupted by periodic machining operations to give the part its final shape (Fig. 6a). UAM is a sheet lamination process, unlike the other methods discussed in this review which are free-form processes. The feed material for UAM is foils with thicknesses on the order of a few hundred microns.[55–57] The ultrasonic vibrations are generated by a low- (1 kW to 2 kW) or high-power (up to 9 kW) transducer and delivered to the foil surface by a sonotrode that vibrates perpendicularly to the build direction. The sonotrode has a rough surface that creates microasperities on the foil surface prior to the placement of the next foil. The high-frequency vibrations and the normal force impose severe plastic deformation between the foils with strain rates as high as 10^4 s^{-1} to 10^5 s^{-1}. Bonding is achieved as a result of the collapse of the microasperities and the severe plastic deformation at the interface.[58,59] Unlike high-temperature consolidation methods, which typically lead to thermal reduction of the oxide layer and subsequent metallurgical bonding, UAM relies on mechanical disruption of the oxide layers between the asperities of the foils due to the scrubbing motion induced by the ultrasonic vibrations followed by dynamic shearing to facilitate metallic bonding.[60] For metallurgical bonding to occur, breakage of the oxide layer and collapse of the asperities on the surface by plastic deformation to bring the metal surfaces into close contact are needed. Because melting is not a mechanism for joining in this technique, controlled atmospheres are not required.

The strength of the ultrasonically manufactured part, especially along the build direction, is predominantly controlled by the porosity, the presence or lack of continuous metallurgical bonding, and the oxide breakage at the interface. Overlapping and staggering of the foils can minimize or prevent void formation at the foil junctions and improve the mechanical properties by preventing alignment of the seams (Fig. 6b). The degree of overlap must be minimal to avoid accumulation of material and subsequent nonuniformity of the build surface.[55]

Porosity at the joining interfaces occurs due to insufficient metal plastic flow and shear, leading to discontinuous metallurgical bonding. The interface strength can be improved by tuning processing parameters, which requires optimization for each alloy. The main processing parameters that dictate the resulting microstructure and properties are the ultrasonic amplitude (5 μm to 50 μm), applied

normal force (0.5 kN to 10 kN), travel speed of the sonotrode (up to 50 mm/s), texture of the sonotrode (R_a 4 μm to 15 μm) and substrate preheat temperature (up to 150°C). Increasing the ultrasonic amplitude, transducer power, normal force, or preheat temperature and decreasing the travel speed of the sonotrode improve the bonding strength between the foils and reduce the interfacial voids.[61] The surface roughness of the foils as well as the sonotrode roughness have also been found to enhance the interface strength, as larger asperities exert greater plastic deformation under ultrasonic scrubbing, leading to better metallurgical bonding.[55]

A significant advantage of UAM is the ease of manufacturing laminar composites by joining dissimilar materials without melting at the interface. Combining a high-strength alloy, such as steel, with lightweight and ductile metals, such as aluminum alloys, with minimal or no formation of brittle intermetallics at the interface presents a critical advantage for automotive and aerospace industries.[12,62,63]

Additive Friction Stir Deposition (AFSD)

Another MD-AM concept is consolidating metals by bonding through vigorous friction by rubbing or rotation, instead of high-frequency ultrasonic vibrations as in UAM. There are a number of variations of additive manufacturing processes that employ this principle of consolidation through friction, as described and discussed in detail by Palanivel and Mishra.[64] In this review, we focus on additive friction stir deposition (AFSD).

AFSD is a thermomechanical additive process in which a feed material, in either rod or powder form, is delivered through a hollow shoulder. The shoulder rotates and generates heat through friction, which softens the filling material and causes it to bond to the substrate surface (Fig. 7). This is a relatively new process that is inspired by a sheet lamination AM method, i.e., friction stir additive manufacturing (FSAM), in which the rotating
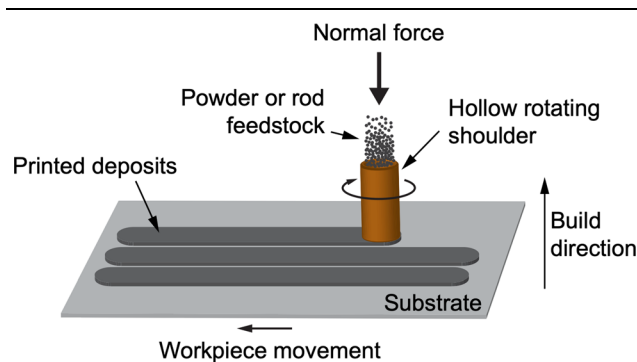
Fig. 7. Schematic of AFSD. A hollow rotating shoulder is fed by powder or rod feedstock and deposits material onto the substrate, applying high shear and normal forces.

shoulder, rather than a hollow core, has a pin that is plunged into stacked metal sheets, cladding them as it traverses the surface. In AFSD, the rotational motion in conjunction with a normal force promotes heating at the material–base plate interface due to friction, which "softens" and severely deforms the feedstock material and creates metallurgical bonding, first with the base plate and subsequently with the previous layer. The heat generated by friction is reported to go up to 0.6 to 0.9 times T_m,[65] which requires tight control of the processing parameters to avoid exceeding the melting temperature. The strain rate that the material experiences is reported to be approximately 1 s^{-1} to 100 s^{-1},[65] a few orders of magnitude lower than in UAM. Despite the high temperatures reached during the process, a controlled atmosphere is not required as the heating is only local. This also makes implementation of on-site repair through AFSD possible. Another advantage of AFSD is that the process allows deposition of multiple materials, enabling the manufacture of bulk, homogeneous metal-matrix composites such as Al-SiC.[66]

The material flow in the friction zone is the key aspect that determines the bonding, microstructure, and mechanical properties. The processing parameters that control the material flow and heat generation in the work area, commonly referred to as the "stir zone," are tool parameters (geometry, rotational speed, traverse velocity, and offset distance), filler feed rate, substrate properties, and cooling media.[64,67] It is argued that the temperature profile within the stir zone in AFSD is different from that in FSAM due to the way the heat is generated and exchanged with the surroundings.[64,65] As a newly developing process, there are not many systematic studies on the relationship between the processing parameters and final properties.

FSAM has attracted attention from the aerospace industry (specifically from Airbus and Boeing), since it offers scalability and the ability to build lightweight structures from reactive alloys based, e.g., on aluminum.[64] Although FSAM has been widely researched and applied, only a limited number of AFSD studies have been reported in literature. Al[68] and Mg[69] AFSD builds from powder feed and Inconel 625[70] and AISI 310[71] stainless steel from a solid rod feed are among the first examples. In addition to these academic reports, MELD Manufacturing Corporation has demonstrated AFSD of low-alloy and stainless steels, Al-, Mg-, Ti-, and Ni-based alloys, in addition to Al- and Cu-based metal-matrix composites.[72]

Cold Spray Additive Manufacturing (CSAM)

The third solid-state additive manufacturing process that establishes bonding through MD is cold spray additive manufacturing (CSAM), which relies on supersonic impact of powder particles onto a substrate. A powder feedstock, carried by a cold
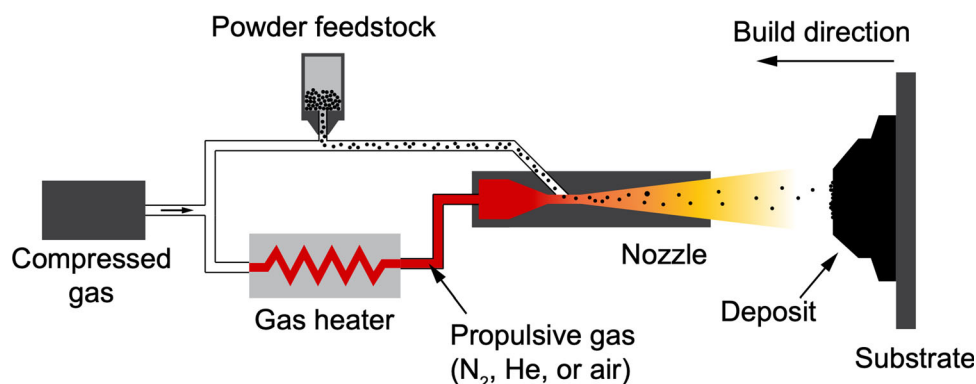
Fig. 8. Schematic of CSAM. Powder feedstock is accelerated by hot propulsive gas and delivered through a nozzle onto the substrate with supersonic velocity.

compressed gas, is accelerated through a heated propulsive gas (25°C to 1000°C), typically nitrogen, helium, or air, to a supersonic velocity toward a substrate[13] (Fig. 8). This is a line-of-sight process where the kinetic energy of the powder particles is mostly converted into their plastic deformation upon impact. The impact results in breakage of the surface oxide layers and severe plastic deformation, leading to metal jetting, characterized by an intense outward material flow (Fig. 9c),[16,73] thus facilitating bonding. Mechanical interlocking between the powder particle and the crater it creates upon impact has also been reported to contribute to bonding.[74] Although cold spray was originally developed as a coating process in the 1980s, it has become an emerging additive manufacturing technology in the past few years.[13]

To establish strong bonding and achieve high-efficiency deposition, the speed of the powder particles must exceed a critical impact velocity. The critical velocity for a material is a function of the material properties of the powder and substrate (density, ductility, strength, shock and thermal properties, and preheating temperature) and the impact parameters (powder size, impact angle, and substrate and particle initial temperatures); For example, the critical velocities for aluminum, nickel, copper, and zinc, for a given powder–substrate configuration, lie in the order Al > Ni > Cu > Zn from highest ($\sim$ 800 m/s) to lowest ($\sim$ 500 m/s). Studies have also showed that the process demands a higher operation velocity for alloys with high melting point and strength, as the critical velocity for bonding is higher; For example, Ti-6Al-4V and Inconel 718 require impact velocities above 1000 m/s and 700 m/s, respectively, while softer alloys such as Cu bond just above 500 m/s.[16,75,76] It has also been found that powders with larger particle size have lower critical velocities, due to the greater heat generation by virtue of their higher kinetic energy.[77] While the powders used in CSAM builds are typically spherical with sizes between 20 μm and 50 μm,[73,78–82] low-cost sponge-like irregular

titanium powders have also been shown to facilitate densification by collapsing at the moment of impact.[83]

The powder particles are brought to their critical impact velocity by using appropriate propulsive gas parameters, where higher gas temperature and pressure and lower gas molecular weight lead to higher particle velocities.[84] Helium, though expensive, yields higher deposition efficiency and stronger bonding, in turn improving the density and ductility of the build compared with counterparts cold-sprayed using nitrogen.[73,80,84,85] The poor mechanical properties and brittleness of nitrogen-sprayed Cu deposits were shown to improve with postspray annealing.[75] The deposit strength and density were also found to increase with increasing gas temperature and spray angle.[86] Other parameters that affect the deposit quality in CSAM parts include the powder feed rate, nozzle traverse speed, standoff distance, scanning step, and nozzle trajectory.[13] As in other solid-state additive manufacturing methods that do not involve high-temperature oxide reduction, the surface oxides play a significant role in the deposit quality and microstructure. Powders with higher oxygen content have been found to reduce the deposition efficiency.[84]

COMPARATIVE ANALYSIS OF SOLID-STATE ADDITIVE MANUFACTURING TECHNIQUES

Flexibility in Terms of Metals and Alloys Suitable for the Processes

The type of metallurgical bonding mechanism can be considered to be one of the critical factors dictating the metals and alloys that are suitable for a given solid-state AM technique; For example, high-hardness alloys such as tool steels and metals that are susceptible to rapid strain hardening are challenging for AM methods that rely on MD, since they require much larger force for deformation bonding and may be susceptible to embrittlement during the process. A summary of processible materials and examples for each technique is
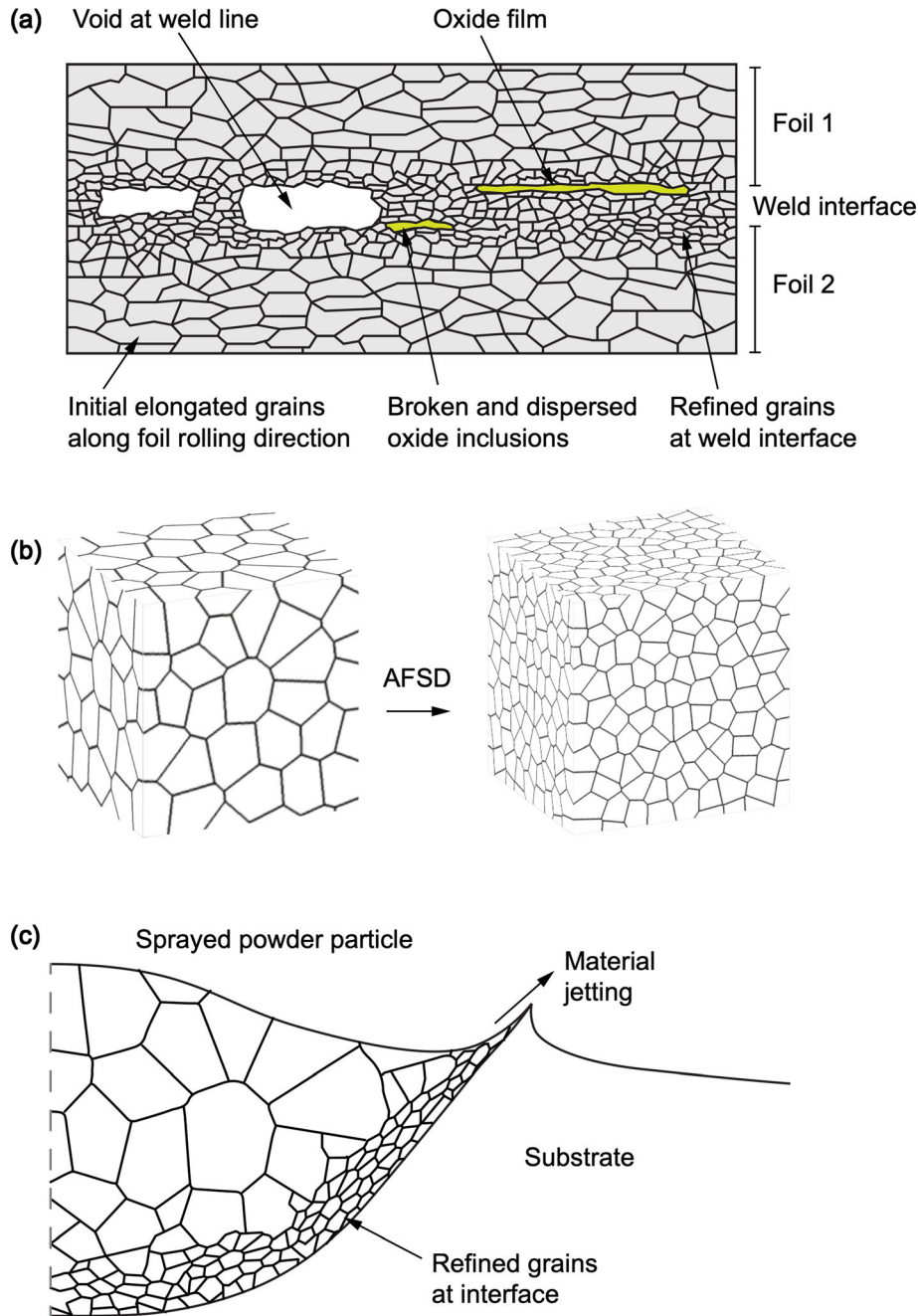
Fig. 9. Schematic depiction of microstructures resulting from MD-AM methods: (a) UAM weld line with refined grains and examples of void and oxide defects, (b) AFSD grain size distribution before and after the process, with grains refined and equiaxed in all orientations, (c) CSAM powder particle during impact, showing refined grains on the impact interface and material jetting.

summarized in Table I. The majority of the literature on UAM focuses on Al alloys,[55,87–92] while fewer publications cover UAM of low-alloy and stainless steels,[57,93] Cu,[60] and bulk metallic glasses.[94] Among steels, UAM is suitable for relatively soft austenitic steels or steels that undergo softening by austenitic transformation during the process.[62] Another limitation on the materials that can be manufactured by UAM is that high-hardness steels and nickel tend to stick to the sonotrode, which can be remedied by tooling

improvements.[12,62] On the other hand, multimaterial printing such as layered or cellular composites[62,63,95] and metallic substrate with embedded electronics[96] is possible using UAM due to its low processing temperatures.

Similarly, the friction-based AM literature is largely limited to relatively soft alloys, as listed in "Additive Friction Stir Deposition (AFSD)" section. One material class that stands out in the list of friction stir AM materials is Mg-based alloys, which are attractive for applications that require light weight and high

Table I. Summary of processible materials and examples of six solid-state AM techniques.

Class	Method	Processible materials	Special material capabilities	Common examples
Sinter-based AM	BJAM	Any powdered material, including ceramics. Hard and brittle materials can be processed	Ceramic- and metal-matrix composites through infiltration	17-4PH, 316L, 304SS, Ti6Al4V, Inconel 625 and 718, Cu, Al_2O_3, Zr_2O_3, WC–Co
Sinter-based AM	MEAM	Any powdered material, including ceramics. Hard and brittle materials can be processed	Multimaterial printing Ceramic- and metal-matrix composites	17-4PH, 316L, H13, A2, D2 tool steels, Inconel 625, Cu, WC–Co
Sinter-based AM	SPAM	Any powdered material, including ceramics. Hard and brittle materials can be processed	Multimaterial printing Ceramic- and metal-matrix composites	Ti6Al4V, CP Ti, 17-4PH, 316L, Cu, Al_2O_3, ZrO_2
MD-AM	UAM	Mostly ductile metals and alloys	Joining dissimilar materials Embedded sensors and electronics	Al alloys, ductile steels
MD-AM	CSAM	Mostly ductile metals and alloys which do not shatter or melt under supersonic impact conditions before exhibiting severe plastic deformation	Small-scale electronic and antenna parts	Cu, Al, Inconel 625, Ti6Al4V, bronze
MD-AM	AFSD	Mostly ductile metals and alloys	Homogeneous metal-matrix composites	Mg and Al alloys, Inconel 625

strength. This hexagonal close-packed (HCP)-structured alloy, due to its limited number of slip systems, has low ductility and fracture toughness, which can be improved through grain refinement. Rolling or forging to achieve grain refinement is not feasible for complex-shaped AM geometries, in addition to the formation of unfavorable texture that imposes anisotropy. FSAM and AFSD have been shown to provide grain refinement while building complex 3D structures, which makes it possible to manufacture Mg-based alloy structures with improved ductility and toughness.[69] Another advantage of these AM methods is that manufacturing of homogeneous, fine-grained metal-matrix composites is relatively easy, although process improvements that address tool wear and hindrance of metal flow by the ceramic reinforcement particles is still needed.[66]

Cold spraying of a variety of metals and alloys including Al-, Cu-, Ti-, and Ni-based alloys is described in literature. A limitation that pertains to CSAM is that a metal or alloy that melts or shatters before exhibiting severe plastic deformation and jetting cannot be bonded using CSAM.[97] Another concern is that alloys that have low thermal conductivity (e.g., Ti and its alloys) and low melting point, as well as metallic glasses may exhibit local melting at the interfaces if the impact velocity and temperature are not well tuned.[16] In summary, MD-AM methods are largely limited to relatively ductile materials.

As briefly described in previous sections, solid-state AM methods that rely on sintering are more flexible in terms of the alloys they can process compared with MD-AM techniques. The ability to utilize powders applied in the more mature MIM technology allows sinter-based AM technologies to draw on a large number of different materials. Unlike MD-AM methods that can operate under normal atmospheric conditions, for sinter-based processes, a controlled atmosphere in the furnace is necessary to avoid oxidation of the powders at high sintering temperatures. This makes sinter-based AM methods challenging for reactive alloys that require a sintering environment with extremely low oxygen and water vapor partial pressure, such as Al- and Ti-based alloys. On the other hand, materials with high hardness such as tool steels, maraging steels, W-heavy alloys, precipitation-hardening steels, hardmetals, and ceramics can easily be manufactured using sinter-based AM methods.[26,47,48]

One commonly overlooked difference between MD- and sinter-based AM methods is the function and limitations of the substrate or base plate. The advantage of sinter-based additive manufacturing methods is that there is no specific requirement on

the base plate other than being compatible with the binder and allowing the build material to stick to the base plate and then be separated without tooling once the printing is completed. On the other hand, the base plate is an active component of MD-AM processes, since it counteracts the forces applied throughout the process. In most MD methods, the material, temperature, and pretreatment of the base plate are critical for the quality of the manufactured part. In friction-based AM, although the substrate material does not have to be the same as the deposit, their strengths and thermal properties should not be drastically different from the build material to ensure good bonding.[65] The residual stress in the build after CSAM has been found to vary significantly depending on the substrate properties and its pretreatment. The thermal residual stress is directly proportional to the difference between the coefficients of thermal expansion of the build material and the substrate.[98] It should also be considered that using a substrate made of a different material than the build material may cause differences in the microstructure and properties as a function of distance from the substrate due to the difference in the thermal and mechanical properties with the build material. The necessity of good bonding between the substrate and the build material also requires a postmanufacturing machining operation to separate the substrate from the build, which is not required after most sinter-based AM methods due to their ability to print a separation layer in between. For MEAM-type processes, often a raft made of the same material is printed directly onto the polymer substrate, which can be easily separated after printing. In the case of BJAM, the substrate is the loose powder on which the part is printed, and which is removed during the depowdering stage. In the case of SPAM, although the substrate used is often metallic, a relatively thin sheet may suffice, as the material deposited during the process is at a very low temperature. The key difference between sinter- and MD-based processes is the degree of bonding between the build substrate and the actual part material that is first laid down on top of the substrate. In the case of MD-based processes, often a fairly strong metallurgical bond is established, while in sinter-based processes, the bonding is extremely weak, thus allowing easy separation of the printed material from the substrate.

Dimensional Accuracy, Resolution, and Geometry Limitations

Attaining dimensional accuracy and a reasonably high resolution are critical to net-shape manufacturing through AM processes. While high-strain-rate AM methods produce parts with final dimensions, the printed parts in sinter-based methods have densities around 50% to 60% of the final material density and undergo significant shrinkage

during sintering. The amount of shrinkage typically varies between 13% and 20% depending on the green density, powder characteristics, part geometry, and size. Understanding and control of the shrinkage during sintering are critical to achieving accurate final parts. Dilatometry is a good way of assessing the shrinkage for a given thermal sintering profile and is widely used for assessing the scaleup factors (the amount of oversizing of the printed part to account for the sintering shrinkage to achieve the final dimensions). Another factor that must be accounted for when determining the scaleup factor is that the shrinkage may also be higher along the build direction (Z-axis) due to gravity, especially in the case of heavy parts, high-temperature creep, and anisotropy of the printed layers. Also of importance in sinter-based processes is the frictional drag between the sintering substrate that the part (in some instances, the sintering raft) is subjected to during the sintering process, as high friction can lead to differential shrinkage, resulting in distortion and/or cracking of the part.

The ability to print fine features is another critical capability expected from AM methods. Comparing the current state of the solid-state technologies discussed in this review, sinter-based methods are reported to provide the highest resolution, typically below 100 μm (Table II). Currently, CSAM and AFSD are limited to millimeter-level resolution, while UAM can achieve micron-level resolution thanks to the machining step. Complex geometries that have fine and unsupported features generally lie beyond the capability of MD-based processes due to the relatively high forces used to attain bonding. To achieve these features, postmanufacturing machining are often employed.[12,13,64] Buckling under large tool forces is another factor in AFSD, FSAM, and UAM that makes building of tall, high-aspect-ratio parts challenging.[65] Cold spray AM of curved and angled geometries requires a careful trajectory design, since the curvature and angles in the part or substrate geometry change the standoff distance between the nozzle and the surface, and the spray angle, which are critical parameters for the deposition efficiency and deposit quality.[13,99]

A notable advantage of MEAM techniques is that they can build parts with a large variety of features, such as overhangs, enclosed cavities, and cooling channels, in a single process by printing an inert separation layer between the part and the support, which will not sinter or react with the build material. Smaller enclosed cavities, such as the internal structure shown in Fig. 4, can be printed without the need for a support, by benefiting from bridging of the viscous extrudate over small gaps. Larger enclosed cavities, on the other hand, require supports that are printed fully from ceramic interface material. The interface material that fills the void and provides support to the enclosed volume becomes loose powder during sintering, since the sintering temperature is too low for the ceramic to

Table II. Practical characteristics of the six solid-state AM methods covered in this review.

Class	Method	Build volume dimensions (cm)	Resolution	Factors controlling resolution	Speed	References
Sinter-based AM	BJAM	Up to $80 \times 50 \times 40$	$< 50 \ \mu m$	Powder size, binder droplet size and spacing, layer height	12,000 cm^3/h	[11,25,26]
Sinter-based AM	MEAM	Up to $30 \times 30 \times 20$	$50 \ \mu m$ to $220 \ \mu m$	Nozzle and powder size	16 cm^3/h	[26,48]
Sinter-based AM	SPAM	$20 \times 30 \times$ (not given)	$< 100 \ \mu m$	Screen aperture design, paste viscosity	100 cm^3/h to 1000 cm^3/h	[50]
MD-AM	UAM	$180 \times 180 \times 160$	$25 \ \mu m$	Machining	10 cm^3/h	[12,101]
MD-AM	CSAM	$\varnothing 35 \times 30$	6 mm	Powder size, nozzle scan speed	600 cm^3/h	[100]
MD-AM	AFSD	$150 \times 150 \times 150$	10 mm	Tool geometry	1000 cm^3/h for Al 80 cm^3/h for Inconel 625	[65,70]

sinter. This loose powder is then shaken out through a small opening, leaving an enclose void behind. Carefully designed temporary support structures that do not belong to the part can support the part throughout printing, debinding, and sintering and then be easily removed from the part by hand, i.e., without tooling. This also enables manufacturing of articulating assemblies in a single process.[26] Screen printing is another sinter-based AM that has the capability of printing cavities and overhangs.[50]

While UAM and AFSD can process the largest build volumes, the speed of the BJAM and SPAM processes makes them suitable for high-volume mass production (Table II).

Microstructure

The bonding mechanism and temperature profile in solid-state AM methods also dictate the resulting microstructure. A major distinction between the two main categories of solid-state AM methods is the nature and uniformity of heat generation during part building. Table III summarizes the thermal and microstructural changes that occur in the build during each process. Sinter-based methods employ uniform external heating during sintering, which generally promotes a relatively uniform microstructure throughout the part. Atomic diffusion is the main bonding mechanism. To achieve the desired final density, parts must be exposed to high temperatures (usually greater than 75% of the melting point of the metal) during sintering. A possible process-related alteration in microstructure may be grain coarsening during sintering if the

temperature profile is not designed properly. Since the parts printed via sinter-based AM are typically not subjected to any external stress prior to or during sintering, the resulting microstructure is dictated primarily by the starting powder characteristics, print defects, chemistry, and sintering conditions. Voids caused by print defects are typically large and cannot be eliminated by sintering. Typical microstructures comprise equiaxed and uniform grains free of deformation-related texture. Different microstructures can emerge in cases of alloys that tend to form elongated grains (such as some Ti-based alloys), partial liquid-phase sintering, formation of grain boundary phases, second-phase precipitation, or abnormal grain growth that may occur during sintering at high temperatures.[28,30]

In contrast, MD-AM methods cause local adiabatic heating and grain refinement due to severe plastic deformation and subsequent recrystallization. The temperature rise is typically local at the interfaces, where material deposition or joining occurs due to both friction and plastic deformation. It is also a function of the build material and the substrate's thermal properties. In UAM, the temperature rise between the layers under the sonotrode has been found to increase with increasing amplitude and alloy shear strength (for example, Cu heats up more than Al).[58] Adiabatic heating that occurs due to high-strain-rate deformation has been found to prevent the material from strain hardening, but localized strain can cause void formation that leads to brittle cracking at the laminate interfaces.[56] While the extent to which Al and Cu

Table III. Thermal and microstructural alterations that occur in parts produced through the solid-state AM methods covered in this review.

| Class	Method	Maximum temperature	Heating mechanism	Bonding mechanism	Microstructure alteration	Microstructure homogeneity
MD-AM	UAM	0.2 to 0.5 T_m	Local—adiabatic	Severe plastic deformation	Recrystallization Grain refinement Texture	Gradient from refined equiaxed grains at the interface to elongated grains with rolling texture of the foil
MD-AM	AFSD	0.6 to 0.9 T_m	Local—adiabatic	Severe plastic deformation	Dynamic recrystallization Grain refinement	Equiaxed, fine, random in all directions
MD-AM	CSAM	Unknown (typically $< T_m$)	Local—adiabatic	Severe plastic deformation	Adiabatic shear and dynamic recrystallization Grain refinement	Fine grains at the particle interfaces
Sinter-based AM	MEAM	$> 0.75 T_m$	Uniform—external heating	Atomic diffusion (generally following oxide reduction)	Minimal/grain coarsening	Equiaxed in all directions (except for some cases, see text)
Sinter-based AM	BJAM	$> 0.75 T_m$	Uniform—external heating	Atomic diffusion (generally following oxide reduction)	Minimal/grain coarsening	Equiaxed in all directions (except for some cases, see text)
Sinter-based AM	SPAM	$> 0.75 T_m$	Uniform—external heating	Atomic diffusion (generally following oxide reduction)	Minimal/grain coarsening	Equiaxed in all directions (except for some cases, see text) Equiaxed in all directions (except for some cases, see text)
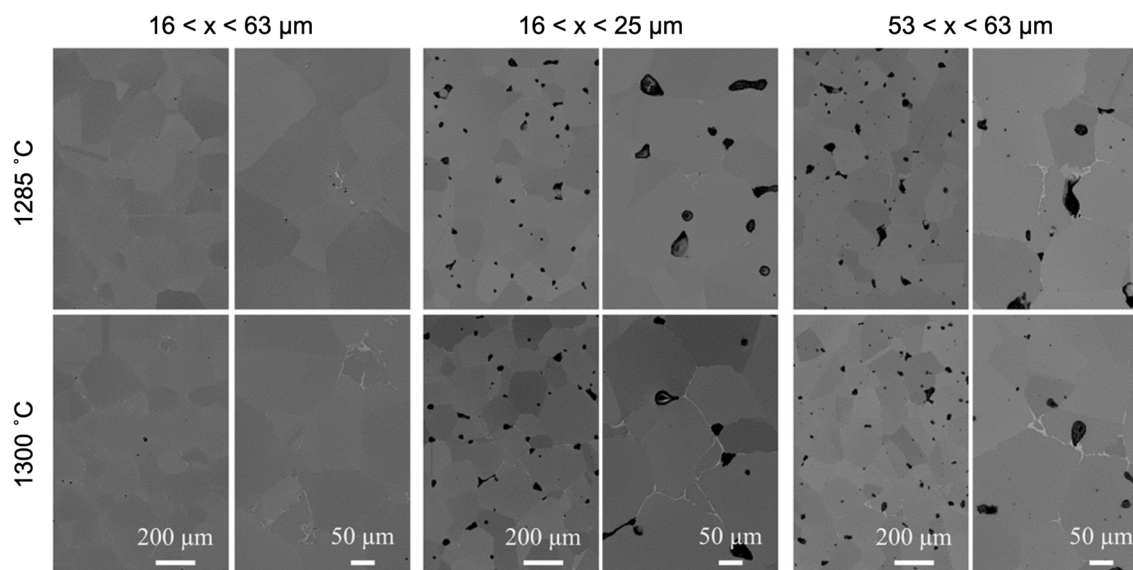
Fig. 10. Microstructures of BJAM Inconel 625 alloy as a function of powder size and distribution and sintering temperature.[30] A larger powder size distribution lead to denser microstructures, while higher sintering temperature resulted in liquid-phase formation on the grain boundaries. Note the equiaxed grains in all microstructures. Although the image is taken from a BJAM build, other sinter-based AM methods lead to similar microstructures under the same powder and sintering conditions. Reprinted from Ref. 30 under the terms of the Creative Commons CC BY-NC-ND license.

heat up locally during processing is typically below 150°C, alloys that undergo phase transformation to a more ductile phase at higher temperatures, such as Ti, require higher heat generation to achieve good bonding.[101] In sheet lamination AM techniques such as UAM and FSAM, elongated grains with a certain rolling texture are typically present in the feed material prior to joining.[88,102] Due to the initial elongated grains along the rolling direction present in the foils with thickness of 100 μm to 150 μm and recrystallized fine grains at the interface with a typical thickness of 10 μm, i.e. an order of magnitude smaller than the foil thickness,[88,91] the resulting microstructure is typically nonuniform in UAM. A representative depiction of typical UAM microstructure that demonstrates the grain size distribution and potential defects such as voids and oxides is shown in Fig. 9a.

The temperatures reached by the material during the process is much higher in FSAM and AFSD compared with UAM. A rolling texture similar to UAM foils is present in the starting metal sheets with millimeter-level thicknesses in FSAM. Severe plastic deformation at the contact between the tool and the part causes recrystallization and grain refinement. In FSAM-processed parts, due to the extent and gradient of frictional heating (0.6 to 0.9 times T_m) through the thickness of the sheet, phases that form along the build direction may also differ.[103] Nanograins at the layer interfaces are reported.[70] Deposition of powder or rod feedstock, instead of sheet welding, i.e., the AFSD process, on the other hand, results in fine, equiaxed, and randomly distributed grains as the whole feedstock goes through the thermomechanical process[68–70,72]

(Fig. 9b). The high temperatures generated during bonding may lead to rapid grain growth in some alloys, which can be mitigated by rapid cooling using liquid N_2 as the cooling medium.[69]

Dynamic recrystallization and grain refinement due to severe plastic deformation are also reported in CSAM builds.[80,85,104] The grain refinement due to deformation and subsequent recrystallization occurs at the level of a single particle. It has been shown that the degree of plastic deformation lessens from the impact surface to the center of the particle, creating a gradient in grain size through the particle cross section[105] (Fig. 10c). Considering that the average powder size used in CSAM is orders of magnitude smaller than the thickness of the foils used in UAM, the degree of microstructural nonuniformity is also much smaller.[106]

The high-strain-rate deformation and localized shear lead to severe local plastic deformation and subsequent recrystallization. This causes a refinement in the grain size with the development of texture after the process.[56,60,88,102,107] An interesting finding regarding the microstructural evolution when dissimilar alloys are joined by UAM is that grain refinement is seen only on the softer side of the interface between alternating softer and harder alloys, due to the greater strain localization in the softer alloy.[63] The resulting texture also differs from that of the same alloy joints due to the difference in adiabatic heating between the two cases. It is also suggested that, to establish complete bonding between alternating dissimilar foils, the pressure applied by the sonotrode should equal the hardness of the softer constituent.[108] Process improvements such as offsetting the angles of foil orientation have
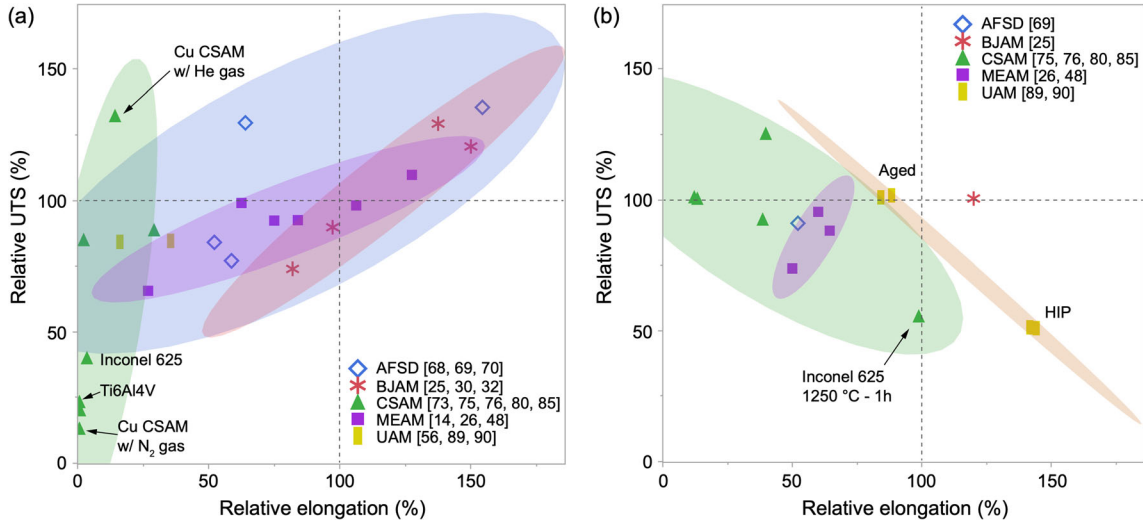
Fig. 11. Ultimate tensile strength and elongation data normalized by wrought values from solid-state AM methods in (a) as-printed or as-sintered state and (b) postmanufacturing treated state. The relative mechanical properties are obtained by normalizing the reported values by wrought properties found in ASM handbooks[110–114] for ease of comparison. Properties in cold-rolled state are taken as reference for the as-built MD-AM alloys, while annealed or aged data are used to normalize the values of the heat-treated mechanical properties depending on the treatment applied. As no cold worked data are available for Al6061 alloy, the values measured on as-received Al6061-H18 tapes in Ref. 89 are taken, while the standard Al6061-T6 properties are taken as a reference for all heat-treated Al6061 data, as this is the most common form of Al6061 available. All data are from samples extracted from builds perpendicular to the build direction. Color version available online.

also been suggested to improve the isotropy on the X–Y plane.[109]

Porosity in the build is a critical factor in the mechanical performance of the part. Sintering powdered metals typically leaves some level of closed porosity in the part, the amount of which depends on the powder size, morphology, distribution, alloy type (diffusivity and self-diffusivity of base and alloying elements), and sintering conditions. The porosity reported in BJAM and MEAM parts varies between 0.4% and 3%[25,28,39] and 2% and 7%,[26,42,48,109] respectively. It is worth noting that the final density can be improved by optimization of the powder size and distribution and the sintering cycle. However, large voids left behind due to print defects are not curable in the sintering cycle. Postsintering containerless HIP is typically used for porosity mitigation. An example of the porosity and grain size distribution as a function of powder size and sintering temperature in BJAM Inconel 625 is shown in Fig. 10.[30] A larger powder size distribution leads to a denser microstructure, while higher sintering temperatures cause liquid-phase formation.

Although voids between the foils welded through UAM are discussed in literature,[87,92] the overall porosity or density is not typically given. CSAM typically leaves 1% to 2% porosity with optimized process parameters and has been shown to improve through postspray heat treatment.[73,76,83,85] Postmanufacturing treatments such as HIP are often used to improve the final density.[80,90] Parts manufactured through AFSD are generally described as "fully dense".[70,101]

In MD-based AM methods, oxides on the feedstock surface are disrupted mechanically, while in sinter-base methods, oxides are reduced thermally at high temperatures. Therefore, the oxides are still physically present in MD builds. Several researchers have shown the presence of a continuous oxide film or round oxide clusters at interfaces after UAM.[87,102] Fragments of broken oxides are detected also in CSAM builds.[79,84] Similarly, some finely dispersed oxides are detected in Al manufactured through AFSD.[68] An interesting effect of residual oxide at the foil interfaces in UAM-built Al is that it impedes grain growth during heat treatment in the seam region, resulting in large differences in grain size along the build direction.[59]

Mechanical Properties and Anisotropy

The ultimate goal of metal additive manufacturing is the ability to fabricate load-bearing components and assemblies with complex geometries without any tooling and preferably without the need for postmanufacturing machining or treatments. The main motivation behind categorizing the solid-state AM methods according to the bonding mechanism is that the nature of the metallurgical bonding and resulting microstructure dictate the mechanical properties of as-built components. In this section, the impact of the microstructural features which form as a result of different material bonding techniques, listed below, on the mechanical behavior is discussed:

- Porosity (shape, size, and distribution)
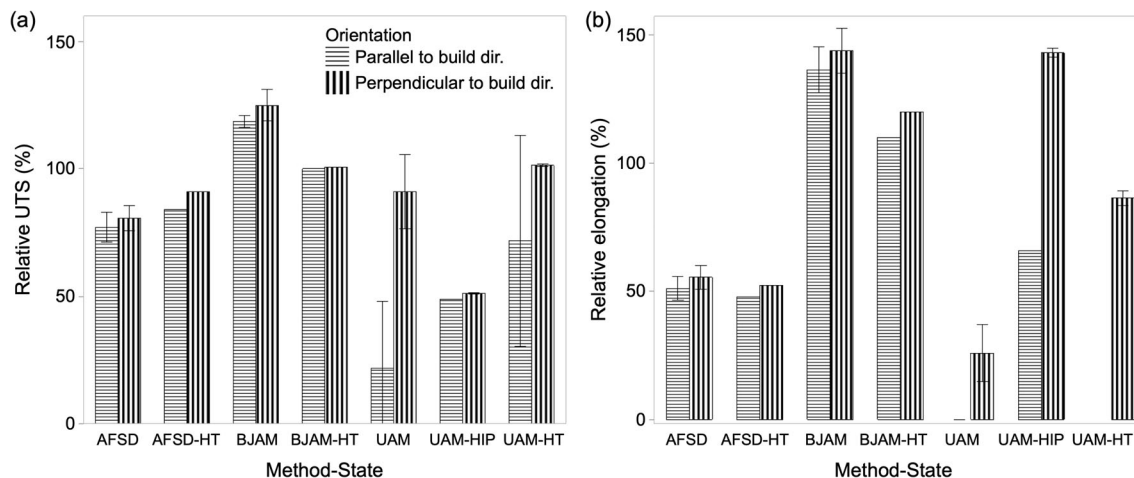- Grain size and distribution

Fig. 12. (a) UTS and (b) elongation percentages normalized by wrought values of the parts in different orientations.[25,56,61,69,89,90,92] HT: heat treated, HIP: hot isostatic pressing. The method of normalization of the mechanical properties is the same as in Fig. 11.

- Texture
- Oxides, precipitates, and impurities
- Residual stress

Figure 11a shows the relative ultimate tensile strength (UTS) and elongation reported in solid-state additively manufactured metals in as-built or as-sintered states perpendicular to the build direction. The relative mechanical properties reported here are normalized by the wrought properties found in ASM handbooks[110–114] for ease of comparison. CSAM- and UAM-processed materials show the lowest elongation, below 50% of the reference, in as-built state. This is attributed to residual stresses and poor metallic bonding between the powder particles in CSAM and voids between the foils in UAM.[56,75] Surface oxides on powder particles are one of the factors that reduce the build strength and ductility, since they inhibit bonding.[84] The lowest strength and elongation points in the CSAM bubble correspond to relatively harder alloys such as Ti-6Al-4V and Inconel 718, compared with cold sprayed Al and Cu samples, which exhibit higher relative UTS and elongation, possibly due to the better bonding provided by their ductility. The large difference in UTS between the Cu builds sprayed using N_2 and He as propeller gas is also significant.

While the data for the heat-treated UAM samples show a significant improvement in both UTS and elongation, CSAM samples still show poor mechanical properties (Fig. 11b). The 100% relative elongation data point in the CSAM bubble is obtained after a heat treatment at around sintering temperature for Inconel 625. Therefore, the high elongation can partially be attributed to sintering. The other heat treatments applied in this dataset are primarily annealing, aging, or HIP, in order to improve mechanical properties by facilitating metallurgical bonding, closing the voids, and relieving stress build up during the processes. Besides enhancing density,

HIP also leads to grain growth due to high temperature, which may in turn be responsible for the strength drop in the UAM samples.[34,90] Hybrid processes that combine technologies that can be used to improve the ductility/plasticity of the CSAM parts, such as friction stir welding of cold spray deposits, are also of recent interest, which is not covered here.[115]

The majority of the tensile samples produced through BJAM, AFSD, and MEAM exhibit high UTS and elongation in both as-built (or as-sintered) and heat-treated states. The majority of the elongation values obtained from as-built AFSD samples are above 50% of their wrought references, possibly due to the relaxation and grain growth effects of the high temperatures generated during the process, which does not occur in CSAM and UAM processes due to their lower temperature. In contrast to CSAM and UAM, parts manufactured through sinter-based AM methods emerge annealed from the furnace. It should be noted some of the alloys (e.g., 316L) processed through MEAM and BJAM are not heat treatable, while others, e.g., 17-4PH and tools steels, are only usable in heat-treated state. Therefore, the aforementioned heat treatments are not employed to modify the as-built properties, but to meet the conventional state of the alloys processed.

Anisotropy

A major challenge in layer-by-layer additive manufacturing is the anisotropy in the mechanical behavior. Specifically, the strength and ductility significantly differ along and perpendicular to the build direction, which is related to the quality of metallurgical bonding between the layers. The bulk mechanical properties along the build direction of solid-state AM materials are rarely reported in literature. Limited data found in literature, only

covering UAM, BJAM, and AFSD processes, are summarized in Fig. 12a and b. Although these data are limited, they provide insight into the aspects of each method that help improve isotropy. Large reductions in tensile strength and brittle fracture have been reported for Al6061 and Al3003 UAM builds when tested along the build direction compared with tensile samples cut perpendicular to the build direction.[56,92] While this is attributed to the oxide layer between the foils in some works,[108] void coalescence due to strain localization at the interface, rather than oxides, is suggested to be the root cause of the poor mechanical properties along the build direction.[56] Another aspect of the process that may lead to poor bonding is the much lower thermal diffusivity along the build direction compared with the foil plane.[91] The anisotropy in strength has been shown to be mitigated through postweld heat treatments, such as annealing and aging to eliminate discontinuities at the interfaces,[55,89] while HIP was been shown to enhance the elongation along the build direction by removing the voids at the interface.[89,90,93] The data reported for BJAM 304 and 316L stainless steels show impressive isotropy in mechanical behavior. While the data are limited, it can be argued that the isotropic mechanical behavior is due to the fact that the powder particles are bound in both the X–Y and Z directions due to the spread of the binder. The isotropy seen in the Mg alloy that was produced via AFSD is a result of randomized material flow created by the moving tool. The filler material is forced into the previous layer, creating diffusion layers with superior bond strength, which leads to good mechanical strength along the build direction.[69]

In some solid-state AM methods, anisotropy does not only occur between the planes that are perpendicular and parallel to the build direction but can also manifest in plane. In CSAM, because powders at the periphery of the spray impact the substrate with a higher angle, the resulting bonding quality varies radially. The bond between neighboring passes was found to cause a drop in tensile properties when tested perpendicular to the gun traverse direction.[82]

Chemistry

Use of carbon-containing binders and interactions of the powder and the binder with the surrounding atmosphere at high temperature render sinter-based AM methods susceptible to chemistry alteration throughout the process. Complete removal of the binder before carbon diffuses into the base metal, especially in the case of steels, is a critical requirement for chemistry control. In two-step debinding processes, complete removal requires prolonged soaks in the debinding fluid and occasional refreshment of the fluid to keep the concentration difference high for removal of the primary binder. Similarly, prolonged soaks at debinding

temperatures in the furnace with a sweep gas to remove the hydrocarbons from the part surfaces is required during thermal debinding of the secondary binder. Depending on the part size, the debinding portion of the postprinting treatments in sinter-based AM methods can take from tens of hours up to several days.[11,41] As oxygen is an effective carbon removal agent, performing thermal debinding under oxygen atmosphere has been shown to accelerate the debinding process, provided that the base metal does not oxidize at the debinding temperatures.[11] Too fast debinding rates can cause distortion and cracking in the parts due to pressure buildup within the part where the generation rate of gaseous hydrocarbons through chain scission is higher than the rate of diffusion of the gaseous species to the surface and subsequent removal. Therefore, a balance must be attained when designing debinding cycles. Alternate binders that can result in faster and cleaner removal have been the topic of ongoing development.

The second critical factor that constitutes a risk of chemistry alteration in sinter-based AM is the sintering atmosphere. An inert atmosphere with a low oxygen and water vapor partial pressure is required to avoid oxygen contamination, reduce oxides on powder surfaces, and facilitate atomic diffusion between them during sintering at high temperature. This is especially challenging for producing reactive metal parts through sinter-based AM methods, as discussed in previous sections. Depending on the alloy type, Ar, H_2, Ar + H_2 blend, N_2, and vacuum environments can provide conditions for successful sintering. Loss of volatile alloying elements such as Cr, Al, and Cu is another risk at high temperatures and in vacuum environments. Another factor that may alter the chemistry is the inherent oxygen content of the powders. The use of powders with high oxygen content can cause a change in the chemistry due to a reaction between carbon and oxygen. Another way in which the chemistry of certain alloys can change is when sintering is carried out in nitrogen or nitrogen-rich atmospheres, where the nitrogen can react with some metals at elevated temperatures to form nitrides.

While sinter-based AM methods require careful process control for chemical stability, especially during sintering, no significant risk of chemistry alteration has been reported in MD-AM methods.

CONCLUSION

Solid-state metal AM technologies offer a variety of capabilities that challenge beam-based methods, such as a large portfolio of processable metals and alloys, unique microstructures, and ease of multi-material manufacturing. It is important to understand the capabilities and limitations of each process to invest in the right technology that meets specific criteria in terms of the metal/alloy of

interest, speed, scale, resulting properties, and need for postprocessing treatments. Having reviewed the current literature on various solid-state metal AM processes, we can summarize the significant trends which we have observed as follows:

- The bonding mechanism is the critical aspect that dictates the processible materials, resulting properties, as well as speed and efficiency of the process.
- The capability to additively manufacture relatively soft and reactive metals and alloys is the strength of mechanical deformation-based processes, while these alloys remain challenging for sinter-based techniques due to high reactivity at sintering temperatures. Inversely, processing harder alloys is more challenging for MD-AM than for sinter-based AM, due to the difficulties associated with mechanical deformation of hard alloys.
- While grain refinement is commonly reported after MD-AM processing, due to severe plastic deformation followed by dynamic recrystallization, sinter-based AM is generally more prone to grain growth due to prolonged exposure to high temperatures during sintering.
- Limited available data suggest that, compared with sinter-based methods, as-built mechanical properties are typically poor in MD-AM processed alloys, which can be improved through postprocessing treatments. The directional nature of most solid-state AM techniques often causes anisotropy, which can only be mitigated by ensuring strong metallurgical bonding not only perpendicular to but also along the build direction. From the limited data available, AFSD and BJAM stand out as the two solid-state AM methods that are capable of achieving isotropic bonding strength in as-built state. More data are needed to confirm this observation.

Although each process has its challenges, most of these technologies are relatively new and rapidly improving with the dynamic research and development environment provided by research institutions and commercial entities. Efforts towards new alloy development for specific solid-state AM techniques and improving bonding quality to achieve good mechanical properties and isotropy will enlarge the vision for solid-state additive manufacturing.

REFERENCES

1. H. Lee, C.H. J. Lim, M.J. Low, N. Tham, V.M. Murukeshan, and Y.J. Kim, *Int. J. Precis. Eng. Manuf. Green Technol.* 4, 307 (2017).
2. T. DebRoy, H.L. Wei, J.S. Zuback, T. Mukherjee, J.W. Elmer, J.O. Milewski, A.M. Beese, A. Wilson-Heid, A. De, and W. Zhang, *Prog. Mater Sci.* 92, 112 (2018).
3. W.E. Frazier, *J. Mater. Eng. Perform.* 23, 1917 (2014).
4. P.K. Gokuldoss, S. Kolla, and J. Eckert, *Materials (Basel)* 10, 672 (2017).
5. W.E. King, A.T. Anderson, R.M. Ferencz, N.E. Hodge, C. Kamath, S.A. Khairallah, and A.M. Rubenchik, *Appl. Phys. Rev.* 2(4), 041304 (2015).
6. Z.C. Eckel, C. Zhou, J.H. Martin, A.J. Jacobsen, W.B. Carter, and T.A. Schaedler, *Science* 351, 58 (2016).
7. H.L. Tekinalp, V. Kunc, G.M. Velez-Garcia, C.E. Duty, L.J. Love, A.K. Naskar, C.A. Blue, and S. Ozcan, *Compos. Sci. Technol.* 105, 144 (2014).
8. A. Kover, GE Reports, Transformation in 3D: how a walnut-sized part changed the way GE aviation builds jet engines (2017). https://www.ge.com/reports/transformation-3d-walnut-sized-part-changed-way-ge-aviation-builds-jet-engines/. Accessed March 2020.
9. X. Gong, T. Anderson, and K. Chou, *Manuf. Rev.* 1(2), 507 (2014).
10. T. Mukherjee, J.S. Zuback, A. De, and T. DebRoy, *Sci. Rep.* 6, 1 (2016).
11. M. Ziaee and N.B. Crane, *Addit. Manuf.* 28, 781 (2019).
12. A. Hehr and M. Norfolk, *Rapid Prototyp. J.* (2019).
13. S. Yin, P. Cavaliere, B. Aldwell, R. Jenkins, H. Liao, W. Li, and R. Lupoi, *Addit. Manuf.* 21, 628 (2018).
14. J. Gonzalez-Gutierrez, S. Cano, S. Schuschnigg, C. Kukla, J. Sapkota, and C. Holzer, *Materials (Basel)* 11, 840 (2018).
15. M. Nastac, R. Lucas, and A. Klein, in *Proceedings of the 28th Annual International Solid Freeform Fabrication*, Austin, TX, pp. 7–9.
16. W. Li, C. Cao, and S. Yin, *Prog. Mater Sci.* 110, 100633 (2019).
17. E.A. Périgo, J. Jacimovic, F. García Ferré, and L.M. Scherf, *Addit. Manuf.* 30, 100870 (2019).
18. Y. Zhang, L. Wu, X. Guo, S. Kane, Y. Deng, Y.G. Jung, J.H. Lee, and J. Zhang, *J. Mater. Eng. Perform.* 27, 1 (2018).
19. S. Chen, Y. Tong, and P.K. Liaw, *Entropy* 20, 937 (2018).
20. Y. Kok, X.P. Tan, P. Wang, M.L.S. Nai, N.H. Loh, E. Liu, and S.B. Tor, *Mater. Des.* 139, 565 (2018).
21. W.J. Sames, F.A. List, S. Pannala, R.R. Dehoff, and S.S. Babu, *Int. Mater. Rev.* 61, 315 (2016).
22. International and S. Organization for Standardization (ISO): Geneve, ISO/ASTM Int. (2017).
23. R. German, *Sintering: From Empirical Observations to Scientific Principles* (Amsterdam: Elsevier Inc., 2014).
24. C.G. Goetzel, *Treatise on Powder Metallurgy, Four Volumes* (New York: Interscience, 1949).
25. ExOne, https://www.exone.com/en-US/3d-printing-materials-and-binders. Accessed March 2020.
26. Desktop Metal, *Studio and production systems*, https://www.desktopmetal.com/. Accessed March 2020.
27. E. Stevens, S. Schloder, E. Bono, D. Schmidt, and M. Chmielus, *Addit. Manuf.* 22, 746 (2018).
28. A. Mostafaei, E.L. Stevens, E.T. Hughes, S.D. Biery, C. Hilla, and M. Chmielus, *Mater. Des.* 108, 126 (2016).
29. I. Rishmawi, M. Salarian, and M. Vlasea, *Addit. Manuf.* 24, 508 (2018).
30. A. Mostafaei, P.R. De Vecchis, I. Nettleship, and M. Chmielus, *Mater. Des.* 162, 375 (2019).
31. P. Nandwana, A.M. Elliott, D. Siddel, A. Merriman, W.H. Peter, and S.S. Babu, *Curr. Opin. Solid State Mater. Sci.* 21, 207 (2017).
32. T. Do, T.J. Bauder, H. Suen, K. Rego, J. Yeom, and P. Kwon, in *International Manufacturing Science and Engineering Conference* (vol. 51357, p. V001T01A017), American Society of Mechanical Engineers (2018).
33. E. Wheat, M. Vlasea, J. Hinebaugh, and C. Metcalfe, *Mater. Des.* 156, 167 (2018).
34. A. Kumar, Y. Bai, A. Eklund, and C.B. Williams, *Procedia Manuf.* 10, 935 (2017).
35. Z.C. Cordero, D.H. Siddel, W.H. Peter, and A.M. Elliott, *Addit. Manuf.* 15, 87 (2017).

36. M. Doyle, K. Agarwal, W. Sealy, and K. Schull, *Procedia Manuf.* 1, 251 (2015).
37. C.L. Cramer, N.R. Wieber, T.G. Aguirre, R.A. Lowden, and A.M. Elliott, *Addit. Manuf.* 29, 100828 (2019).
38. C.L. Cramer, A.M. Elliott, J.O. Kiggans, B. Haberl, and D.C. Anderson, *Mater. Des.* 180, 107956 (2019).
39. T. Do, P. Kwon, and C.S. Shin, *Int. J. Mach. Tools Manuf.* 121, 50 (2017).
40. Scott Crump, *Apparatus and method for creating three-dimensional objects*, US Patent US 5,121,329 A (1989).
41. R. German and A. Bose, *Injection Molding of Metals and Ceramics* (Princeton: Metal Powder Industries Federation, 1997).
42. Y. Thompson, J. Gonzalez-Gutierrez, C. Kukla, and P. Felfer, *Addit. Manuf.* 30, 100861 (2019).
43. A. Preston, N. Mykulowycz, A.C. Barbati, M.A. Gibson, C.J. Haider, and J. Tobia, *High density 3d printing*, U.S. Patent Application No. 15/953,380 (2018).
44. J. S. Batchelder, *Method for controlled porosity three-dimensional modeling*, US Patent US 5,653,925 A (1995).
45. Clemens Lieberwirth, Arne Harder, and Hermann Seitz, *J. Mech. Eng. Autom.* 7, 79 (2017).
46. C. Lieberwirth, M. Sarhan, and H. Seitz, *Metals (Basel)* 8, 84 (2018).
47. W. Lengauer, I. Duretek, V. Schwarz, C. Kukla, M. Kitzmantel, E. Neubauer, C. Lieberwirth, and V. Morrison, *Euro PM 2018 Congr. Exhib.* (2020).
48. Markforged, https://markforged.com/materials/. Accessed March 2020.
49. A. Bose, C.A. Schuh, J.C. Tobia, N. Tuncer, N.M. Mykulowycz, A. Preston, A.C. Barbati, B. Kernan, M.A. Gibson, D. Krause, T. Brzezinski, J. Schroers, R. Fulop, J.S. Myerberg, M. Sowerbutts, Y.-M. Chiang, A. John Hart, E.M. Sachs, E.E. Lomeli, and A.C. Lund, *Int. J. Refract. Met. Hard Mater.* 73, 22 (2018).
50. M. Dressler, T. Studnitzky, and B. Kieback, *Proc. 2017 19th Int. Conf. Electromagn. Adv. Appl. ICEAA 2017* 476 (2017).
51. J. Pan, G.L. Tonkay, R.H. Storer, R.M. Sallade, D.J. Leandri, and I.E.E.E. Trans, *Electron. Packag. Manuf.* 27, 125 (2004).
52. N. Khader, J. Lee, D. Lee, S.W. Yoon, and H. Yang, *Procedia Manuf.* 38, 163 (2019).
53. M. Jurisch, T. Studnitzky, O. Andersen, and B. Kieback, *World PM 2016 Congr. Exhib.* (2016).
54. Met. AM Spring, *Exentis Group demonstrates industrialisation of its 3D screen printing additive manufacturing technology*, vol. 6, no. 1 (2020).
55. P.J. Wolcott, A. Hehr, C. Pawlowski, and M.J. Dapino, *J. Mater. Process. Technol.* 233, 44 (2016).
56. N. Sridharan, M. Gussev, R. Seibert, C. Parish, M. Norfolk, K. Terrani, and S.S. Babu, *Acta Mater.* 117, 228 (2016).
57. A. Levy, A. Miriyev, N. Sridharan, T. Han, E. Tuval, S.S. Babu, M.J. Dapino, and N. Frage, *J. Mater. Process. Technol.* 256, 183 (2018).
58. M.R. Sriraman, M. Gonser, H.T. Fujii, S.S. Babu, and M. Bloss, *J. Mater. Process. Technol.* 211, 1650 (2011).
59. N. Sridharan, M.N. Gussev, C.M. Parish, D. Isheim, D.N. Seidman, K.A. Terrani, and S.S. Babu, *Mater. Charact.* 139, 249 (2018).
60. M.R. Sriraman, S.S. Babu, and M. Short, *Scr. Mater.* 62, 560 (2010).
61. P.J. Wolcott, A. Hehr, and M.J. Dapino, *J. Mater. Res.* 29, 2055 (2014).
62. C.H. Kuo, N. Sridharan, T. Han, M.J. Dapino, and S.S. Babu, *Sci. Technol. Weld. Join.* 24, 382 (2019).
63. N. Sridharan, P. Wolcott, M. Dapino, and S.S. Babu, *Sci. Technol. Weld. Join.* 22, 373 (2017).
64. R.S. Mishra and S. Palanivel, *Int. J. Addit. Subtractive Mater. Manuf.* 1, 82 (2017).
65. H.Z. Yu, M.E. Jones, G.W. Brady, R.J. Griffiths, D. Garcia, H.A. Rauch, C.D. Cox, and N. Hardwick, *Scr. Mater.* 153, 122 (2018).
66. R.J. Griffiths, M.E.J. Perry, J.M. Sietins, Y. Zhu, N. Hardwick, C.D. Cox, H.A. Rauch, and H.Z. Yu, *J. Mater. Eng. Perform.* 28, 648 (2019).
67. F. Khodabakhshi and A.P. Gerlich, *J. Manuf. Process.* 36, 77 (2018).
68. A. Mukhopadhyay and P. Saha, *J. Mater. Process. Technol.* 281, 116648 (2020).
69. J.R. Calvert, *Microstructure and Mechanical Properties of WE43 Alloy Produced via Additive Friction Stir Technology* (Blacksburg: Virginia Polytechnic Institute and State University, 2015).
70. O.G. Rivera, P.G. Allison, J.B. Jordon, O.L. Rodriguez, L.N. Brewer, Z. McClelland, W.R. Whittington, D. Francis, J. Su, R.L. Martens, and N. Hardwick, *Mater. Sci. Eng. A* 694, 1 (2017).
71. J.J.S. Dilip, G.D.J. Ram, and B.E. Stucker, *Int. J. Rapid Manuf.* 3, 56 (2012).
72. MELD Manufacturing, http://meldmanufacturing.com/. Accessed March 2020.
73. X. Wang, F. Feng, M.A. Klecka, M.D. Mordasky, J.K. Garofano, T. El-Wardany, A. Nardi, and V.K. Champagne, *Addit. Manuf.* 8, 149 (2015).
74. T. Hussain, D.G. McCartney, P.H. Shipway, and D. Zhang, *J. Therm. Spray Technol.* 18, 364 (2009).
75. F. Gärtner, T. Stoltenhoff, J. Voyer, H. Kreye, S. Riekehr, and M. Koçak, *Surf. Coat. Technol.* 200, 6770 (2006).
76. W. Wong, E. Irissou, P. Vo, M. Sone, F. Bernier, J.G. Legoux, H. Fukanuma, and S. Yue, *J. Therm. Spray Technol.* 22, 413 (2013).
77. I. Dowding, M. Hassani, Y. Sun, D. Veysset, K.A. Nelson, and C.A. Schuh, *Acta Mater.* 194, 40 (2020).
78. Z. Cai, S. Deng, H. Liao, C. Zeng, and G. Montavon, *J. Therm. Spray Technol.* 23, 354 (2014).
79. C. Chen, Y. Xie, R. Huang, S. Deng, Z. Ren, and H. Liao, *Mater. Lett.* 210, 199 (2018).
80. C. Chen, Y. Xie, X. Yan, S. Yin, H. Fukanuma, R. Huang, R. Zhao, J. Wang, Z. Ren, M. Liu, and H. Liao, *Addit. Manuf.* 27, 595 (2019).
81. Y. Watanabe, Y. Ichikawa, I. Nonaka, and H. Miura, *14th Int. Conf. Electron. Mater. Packag. EMAP 2012* 4 (2012).
82. K. Yang, W. Li, X. Guo, X. Yang, and Y. Xu, *J. Mater. Sci. Technol.* 34, 1570 (2018).
83. D. MacDonald, R. Fernández, F. Delloro, and B. Jodoin, *J. Therm. Spray Technol.* 26, 598 (2017).
84. W.Y. Li, C.J. Li, and H. Liao, *Appl. Surf. Sci.* 256, 4953 (2010).
85. W. Ma, Y. Xie, C. Chen, H. Fukanuma, J. Wang, Z. Ren, and R. Huang, *J. Alloys Compd.* 792, 456 (2019).
86. K. Binder, J. Gottschalk, M. Kollenda, F. Gärtner, and T. Klassen, *J. Therm. Spray Technol.* 20, 234 (2011).
87. H.T. Fujii, S. Shimizu, Y.S. Sato, and H. Kokawa, *Scr. Mater.* 135, 125 (2017).
88. S. Shimizu, H.T. Fujii, Y.S. Sato, H. Kokawa, M.R. Sriraman, and S.S. Babu, *Acta Mater.* 74, 234 (2014).
89. M.N. Gussev, N. Sridharan, M. Norfolk, K.A. Terrani, and S.S. Babu, *Mater. Sci. Eng. A* 684, 606 (2017).
90. M.N. Gussev, N. Sridharan, Z. Thompson, K.A. Terrani, and S.S. Babu, *Scr. Mater.* 145, 33 (2018).
91. E. Cakmak, M.N. Gussev, N. Sridharan, M.H. Seren, K. An, H. Wang, and K.A. Terrani, *Mater. Sci. Eng. A* 770, 138 (2020).
92. D.E. Schick, MS Thesis (2009).
93. T. Han, C.H. Kuo, N. Sridharan, L.M. Headings, S.S. Babu, and M.J. Dapino, *Mater. Sci. Eng. A* 769, 138457 (2020).
94. W. Wu, J. Jiang, G. Li, J.Y.H. Fuh, H. Jiang, P. Gou, L. Zhang, W. Liu, and J. Zhao, *J. Non Cryst. Solids* 506, 1 (2019).
95. E.M. Parsons, *Compos. Struct.* 223, 110656 (2019).
96. A. Bournias-varotsis, R.J. Friel, R.A. Harris, and D.S. Engstrøm, *J. Manuf. Process.* 32, 664 (2018).
97. S.C. Hassani-Gangaraj, D. Veysset, and K.A. Nelson, *Phys. Rev. Lett.* (2017).
98. T. Suhonen, T. Varis, S. Dosta, M. Torrell, and J.M. Guilemany, *Acta Mater.* 61, 6329 (2013).
99. M.E. Lynch, W. Gu, T. El-wardany, A. Hsu, and D. Viens, *Virtual Phys. Prototyp.* 8, 213 (2013).
100. Spee3d, https://www.spee3d.com/. Accessed March 2020.

101. Fabrisonic (2020), https://fabrisonic.com/3dprinting/wp-content/uploads/2018/03/FAQ-Design-Guide_S.pdf. Accessed March 2020.
102. R.R. Dehoff and S.S. Babu, *Acta Mater.* 58, 4305 (2010).
103. K. Gangwar and M. Ramulu, *Mater. Des.* 141, 230 (2018).
104. K.H. Kim, M. Watanabe, J. Kawakita, and S. Kuroda, *Scr. Mater.* 59, 768 (2008).
105. C. Lee and J. Kim, *J. Therm. Spray Technol.* 24, 592 (2015).
106. M.R. Rokni, S.R. Nutt, C.A. Widener, V.K. Champagne, and R.H. Hrabe, *J. Therm. Spray Technol.* 26, 1308 (2017).
107. R.J. Friel and R.A. Harris, *Procedia CIRP* 6, 35 (2013).
108. A.A. Ward and Z.C. Cordero, *Scr. Mater.* 177, 101 (2020).
109. J. Gonzalez-Gutierrez, F. Arbeiter, T. Schlauf, C. Kukla, and C. Holzer, *Mater. Lett.* 248, 165 (2019).
110. ASM International Handbook Committee, *ASM Handbook Volume 4E: Heat Treating of Nonferrous Alloys* (2001).
111. J.R. Davis, in *ASM Spec. Handb. Copp. Copp. Alloy.* (2001), pp. 446–452.
112. ASM International Handbook Committee, *ASM Handbook Vol 1: Properties and Selection: Irons, Steels, and High-Performance Alloys* (1990).
113. ASM International Handbook Committee, *ASM Handbook Vol. 2: Properties and Selection: Nonferrous Alloys and Special-Purpose Materials* (2001).
114. H. Avedesian, M. M. Baker, *ASM Spec. Handb.—Magnes. Magnes. Alloy.* (1999).
115. W. Li, C. Cao, G. Wang, F. Wang, Y. Xu, and X. Yang, *Sci. Technol. Weld. Join.* 24, 420 (2019).